

# The Stability of Liquid Hydrocarbon Vapor Sensors Based on SnO<sub>2</sub> Thin Films Modified with Various Catalysts

N. K. Maksimova<sup>a</sup>, B. O. Kushnarev<sup>b,\*</sup>, L. S. Khludkova<sup>a</sup>, A. A. Biryukov<sup>a</sup>,  
E. Yu. Sevast'yanov<sup>a</sup>, and E. V. Chernikov<sup>a,b</sup>

<sup>a</sup> Siberian Kuznetsov Institute of Physics and Technology, Tomsk State University, Tomsk, 634050 Russia

<sup>b</sup> Research and Development Center "Advanced Technologies in Microelectronics," Tomsk State University, Tomsk, 634050 Russia

\*e-mail: kuschnaryow@mail.ru

Received December 22, 2020; revised February 10, 2021; accepted February 23, 2021

**Abstract**—The microstructure, composition, and electrical and gas-sensitive characteristics of sensors based on thin nanocrystalline SnO<sub>2</sub> films with various catalysts deposited on the surface (Pt/Pd, Au) and introduced into the bulk (Au, Ni, Co) are investigated in the modes of constant and pulse heating. Atomic force microscopy and laser Raman spectroscopy are used to study micromorphology and structural defects depending on the composition of nanosized films. It is shown that sensors with Au and Co additives introduced into the volume make it possible to detect vapors of liquid hydrocarbons (on the example of aviation kerosene) at a concentration level of 5 ppm (0.1 of permissible exposure limit) and are characterized by increased stability of parameters during testing under prolonged exposure to vapors, as well as in conditions of varying humidity. Sensors with Au and Co additives in volume and deposited onto the film surface ultrathin two-layer Pt/Pd catalysts demonstrate the fastest response after testing.

DOI: 10.1134/S1063784221070094

## INTRODUCTION

One urgent environmental problem at the present time is the pollution of the atmosphere with vapors of liquid hydrocarbons. The control of aviation fuel leaks at aerodrome and near aerodrome areas requires special attention. The permissible exposure limit (PEL) of aviation kerosene vapors in the air of the working area is 300 mg/m<sup>3</sup>, and exceeding it causes a negative effect on the human body. In addition, high levels of vapors in the air during fuel spills can lead to the formation of an explosive mixture. Continuous monitoring of fuel leaks during storage, transportation, and aircraft refueling requires highly sensitive sensors capable of detecting aviation kerosene vapors at the PEL level and below. Existing control systems use mainly electrochemical or optical sensors and are designed to determine explosive vapor concentrations that are two orders of magnitude higher than the PEL. Semiconductor sensors are also used, which are manufactured mainly using thick-film technology. Their disadvantages include low performance and insufficient stability of parameters during long-term operation [1–3]. Thin films of metal oxide semiconductors are a promising material for the creation of gas sensors. Sensors based on them have a number of advantages, such as high sensitivity to the effects of reducing gases

including vapors of liquid hydrocarbons, low manufacturing costs, and miniaturization.

The gas-sensitive characteristics of sensors based on nanocrystalline metal oxide semiconductors can be controlled by catalytic additives (noble and 3d-metals, rare earth elements) introduced into the bulk and applied onto the surface [4–7]. At the same time, the processes of heterogeneous catalysis on the surface of semiconductors in the presence of active catalysts, which lie at the basis of detection, remain insufficiently studied, as well as the phenomena responsible for the degradation of the parameters of the sensors during long-term tests and under conditions of varying humidity [8–10]. The choice of the composition of the films and the type of catalysts in the volume and on the surface remains empirical. It seems necessary to carry out comprehensive studies of the relationship between the manufacturing technology, composition, microstructure, and properties of metal oxide semiconductors with various catalytic additives for the development of new scientific approaches to the creation of sensors with specified parameters. Earlier [11–13], we showed that the introduction of an Au impurity and additives of 3d transition metals (Ni, Co) into the bulk of thin nanocrystalline SnO<sub>2</sub> films leads to an increase in the response to a number of reducing gases (hydrogen, hydrogen sulfide, ethanol and ace-

tone vapors) and an increase in the stability of the sensor parameters.

In this work, we performed a comprehensive study of the effect of various catalysts deposited on the surface (Pt/Pd, Au) and introduced into the bulk (Au, Ni, Co) of thin nanocrystalline SnO<sub>2</sub> films obtained by magnetron sputtering on microstructure, composition, electrical and gas-sensitive characteristics, and stability with the aim of creating sensors for vapors of aviation kerosene. The physical and chemical processes responsible for the properties of films and their degradation were considered, and ways to increase the stability of the parameters of the sensors during long-term tests and under conditions of varying humidity were determined.

## 1. MATERIALS AND METHODS

SnO<sub>2</sub> films doped with antimony impurity were obtained in an A-500 magnetron (Edwards) by direct current sputtering of a target made of Sn + Sb (0.5 vol %) alloy in an oxygen–argon plasma. Sapphire wafers with a thickness of 150 μm were used as substrates. Antimony in tin dioxide with a rutile structure replaces tin; moreover, most of the Sb has a valence of +5; the impurity creates donor centers in the semiconductor [11] and promotes a decrease in the resistivity of the films to values of 1–10 MΩ in the operating mode, which is necessary in the development of sensors with low noise levels. To introduce gold, nickel, and cobalt into the SnO<sub>2</sub> volume, pieces of these metals were placed on the target surface. The content of additives was controlled by the ratio of the areas of metal pieces  $S_m$  and the sputtered part of the  $S_{Sn}$  target. Dispersed layers of Pt/Pd and Au catalysts were deposited on the surface of the films by the same magnetron sputtering. The features of the sample manufacturing technology are similar to those described in [11–14].

Platinum contacts to the SnO<sub>2</sub> layers and a heater on the back side of the substrate were formed before the deposition of the films. The substrates were heated to a temperature of at least 500°C to ensure high adhesion of platinum during magnetron sputtering by direct current. Then photolithographic engraving of platinum was carried out. Two steps of photolithography were used to form a sensitive layer of a specific size.

The finished samples were annealed in air at a temperature of 450°C for 24 h. Up to 500 sensors 0.7 × 0.7 mm in size with a gas-sensitive film area of 0.3 × 0.3 mm were obtained on a single substrate with a diameter of 30 mm. The wafers were cut into individual elements and, then, electric outlets made of gold wire with a diameter of 50 μm were welded to the contact pads of the sensors (by thermal compression). The samples were assembled in TO-8 metal cases.

The experimental results were compared with the data for Pt/Pd/SnO<sub>2</sub>:Sb films without bulk additives.

Let us introduce the following series numbering and designations for the studied sensors:

(I) Pt/Pd/SnO<sub>2</sub>:Sb;

(II) Au/SnO<sub>2</sub>:Sb, Au, Ni,  $S_{Au}/S_{Sn} = S_{Ni}/S_{Sn} = 3 \times 10^{-3}$ ;

(III) Au/SnO<sub>2</sub>:Sb, Au, Co,  $S_{Au}/S_{Sn} = 6 \times 10^{-3}$ ,  $S_{Co}/S_{Sn} = 9 \times 10^{-3}$ ; and

(IV) Pt/Pd/SnO<sub>2</sub>:Sb, Au, Co,  $S_{Au}/S_{Sn} = 6 \times 10^{-3}$ ,  $S_{Co}/S_{Sn} = 3 \times 10^{-3}$ .

The thickness and microstructure of the films were monitored on a Solver HV atomic force microscope (AFM) from NT-MDT. The required parameters were obtained using the ImageAnalysis software module for processing the images with the \*.mdt format. The elemental composition of the films was analyzed using layer-by-layer Auger electron spectroscopy (AES) on a Shchuna-2 setup (the methodology is described in [13]). The samples with SnO<sub>2</sub>:Sb, Au, Ni, ( $S_{Au}/S_{Sn} = S_{Ni}/S_{Sn} = 3 \times 10^{-3}$ ) and SnO<sub>2</sub>:Sb, Au, Co ( $S_{Au}/S_{Sn} = 6 \times 10^{-3}$ ,  $S_{Co}/S_{Sn} = 9 \times 10^{-3}$ ) films with an area of 10–15 mm<sup>2</sup> were specially prepared for the AES studies. A platinum layer was deposited on the sapphire substrate before the deposition of tin dioxide to prevent the effect of charge accumulation. This method makes it possible to detect all elements (except for hydrogen and helium), the concentration of which is >0.3–0.5 at %.

Raman spectroscopy was used to study the features of structural defects in a nanosized material with various additives and sprayed catalysts. Raman spectra for sensors with a 0.3 × 0.3-mm area of gas-sensitive elements were measured on an inVia confocal Raman spectrometer (Renishaw, United Kingdom) operating in the backscattering mode at room temperature (details of the research technique are presented in [13]).

To study the gas-sensitive properties, the sensors were placed in a 1-L quartz chamber equipped with a fan; clean air was pumped through it, after which the chamber was sealed. The chamber was pumped using two air streams—dried with zeolite and humidified with a bubbler—which made it possible to regulate the humidity of the air entering the chamber. The relative humidity RH was determined using an HIH-4000 capacitive sensor placed in the chamber. The required volume of saturated vapors of TS-1 aviation kerosene was fed into the chamber using Hamilton microsyringes for chromatography. When converting the concentration from mg/m<sup>3</sup> units to ppm, the averaged value of the molecular weight of TS-1  $M = 156$  was used.

The time dependences of the conductivity  $G_0$  and resistance  $R_0$  of the sensors in clean air, as well as  $G_1(R_1)$  when exposed to aviation kerosene vapors, were measured in constant heating and thermal cycling modes using a specially designed stand, which

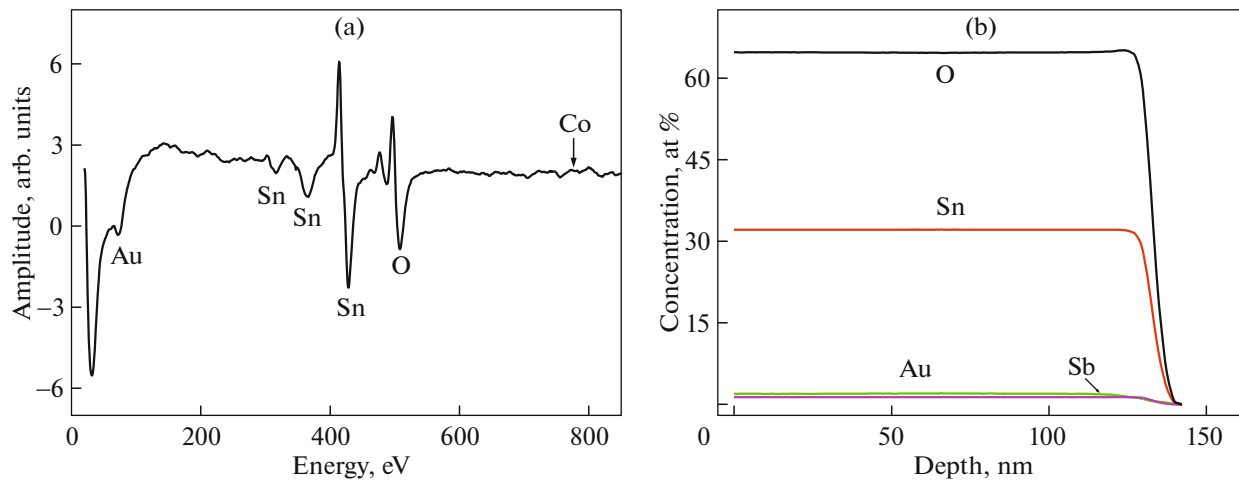


**Fig. 1.** (a) Auger spectra of the  $\text{SnO}_2\text{:Sb}$ , Au, Co film depending on the kinetic energy of electrons at a layer depth of 50 nm; (b) profiles of distribution of the relative concentrations of the detected elements over the film thickness.

made it possible to register  $G_0(t)$  and  $G_1(t)$  at a time interval  $\Delta t = 0.01$  s and to rearrange the temperatures and durations of heating and cooling cycles. The ratio  $G_1/G_0$  was taken as the adsorption response, and response time  $t_r$  was the time of  $0.9G_{st}$  settling, where  $G_{st}$  is the stationary value of conductivity.

In the thermal cycling mode, the response values were measured at the end of the cooling cycles  $S(T_1) = G(T_1)_1/G(T_1)_0$  and heating cycles  $S(T_2) = G(T_2)_1/G(T_2)_0$ . To study the stability of the parameters during long-term operation of the sensors under the influence of kerosene vapor, the concentration dependences of the response were measured every 2–4 days or more (up to 60–90 days) in the concentration range of 5–75 ppm, as well as a response at 15 ppm. The effect of humidity was studied in the range of RH = 6–70%.

## 2. EXPERIMENTAL RESULTS AND DISCUSSION

### 2.1. Characteristics of Thin Films of Various Compositions

The AFM studies showed that the thicknesses of tin dioxide films from different series are in the range of 100–130 nm. The sizes of nanocrystallites vary from  $d_1 = 10$ –15 nm (series (I) and (III)) and 40–50 nm (series (II) and (IV)) to  $d_2 = 100$ –125 nm (series (I) and (II)), and 150–260 nm (series (III) and (IV)). The presence of crystallites with the sizes of  $d_2 = 150$ –260 nm is due to the increased concentration of gold in these films ( $S_{Au}/S_{Sn} = 6 \times 10^{-3}$ ). Earlier [11], it was shown that the addition of gold to the bulk of thin films of tin dioxide promotes the formation of larger crystallites.

According to the results of layer-by-layer AES of  $\text{SnO}_2\text{:Sb}$ , Au, Co, ( $S_{Au}/S_{Sn} = 6 \times 10^{-3}$ ,  $S_{Co}/S_{Sn} = 9 \times 10^{-3}$ ) films (Fig. 1), the relative concentrations of Sn and O correspond to  $\text{SnO}_2$ , the Au concentration is 1.8–1.9 at %, and the Sb concentration is 0.7–0.8 at %. The Co content (Fig. 1a) is at the sensitivity limit of the method, i.e., <0.3–0.5 at %. In the  $\text{SnO}_2\text{:Sb}$ , Au, Ni ( $S_{Au}/S_{Sn} = S_{Ni}/S_{Sn} = 3 \times 10^{-3}$ ) film, the concentration of Au and Ni is below the sensitivity limit of the method; i.e., <0.3–0.5 at %. It should be noted that the AES is a semiquantitative method.

Figure 2 shows the Raman spectra of the studied films of different compositions. The main modes of nanocrystalline  $\text{SnO}_2\text{:Sb}$  and Au/ $\text{SnO}_2\text{:Sb}$  films,  $E_g$  468  $\text{cm}^{-1}$  and  $A_{1g}$  630  $\text{cm}^{-1}$  (Fig. 2a, curves 1, 2), are characteristic of tin dioxide with a rutile structure. It is known [15, 16] that the following modes are active in the Raman spectra for bulk  $\text{SnO}_2$  crystals:  $E_g$  476  $\text{cm}^{-1}$ ,  $A_{1g}$  638  $\text{cm}^{-1}$ , and  $B_{2g}$  782  $\text{cm}^{-1}$ , as well as  $B_{1g}$  123  $\text{cm}^{-1}$ , with  $A_{1g}$  638  $\text{cm}^{-1}$  mode being the most intense. Raman spectra for bulk materials and polycrystalline samples, where the size of particles (grains, agglomerates, clusters, etc.) lies in the nanometer range, differ greatly, and the classical  $E_g$ ,  $A_{1g}$ , and  $B_{2g}$  modes shift and broaden [17].

In the spectra in Fig. 2a, the  $B_{1g}$  123  $\text{cm}^{-1}$  mode is weakly expressed, while the  $B_{2g}$  mode does not appear in the spectrum. In the region from 200 to 350  $\text{cm}^{-1}$ , there are clearly defined peaks with maxima at 248 and 286  $\text{cm}^{-1}$ , which are usually attributed to anomalous ones [16] and associated with IR active  $E_u$  TO- and  $E_u$  LO-modes, respectively. We also note that the maxima at 605 and 725  $\text{cm}^{-1}$  (Fig. 2a, curve 1) are weakly expressed and are represented on the spectrum as “shoulders” of bending. These peaks are probably also related to  $E_u$  TO- and  $E_u$  LO- or  $A_{2u}$  LO-modes. The

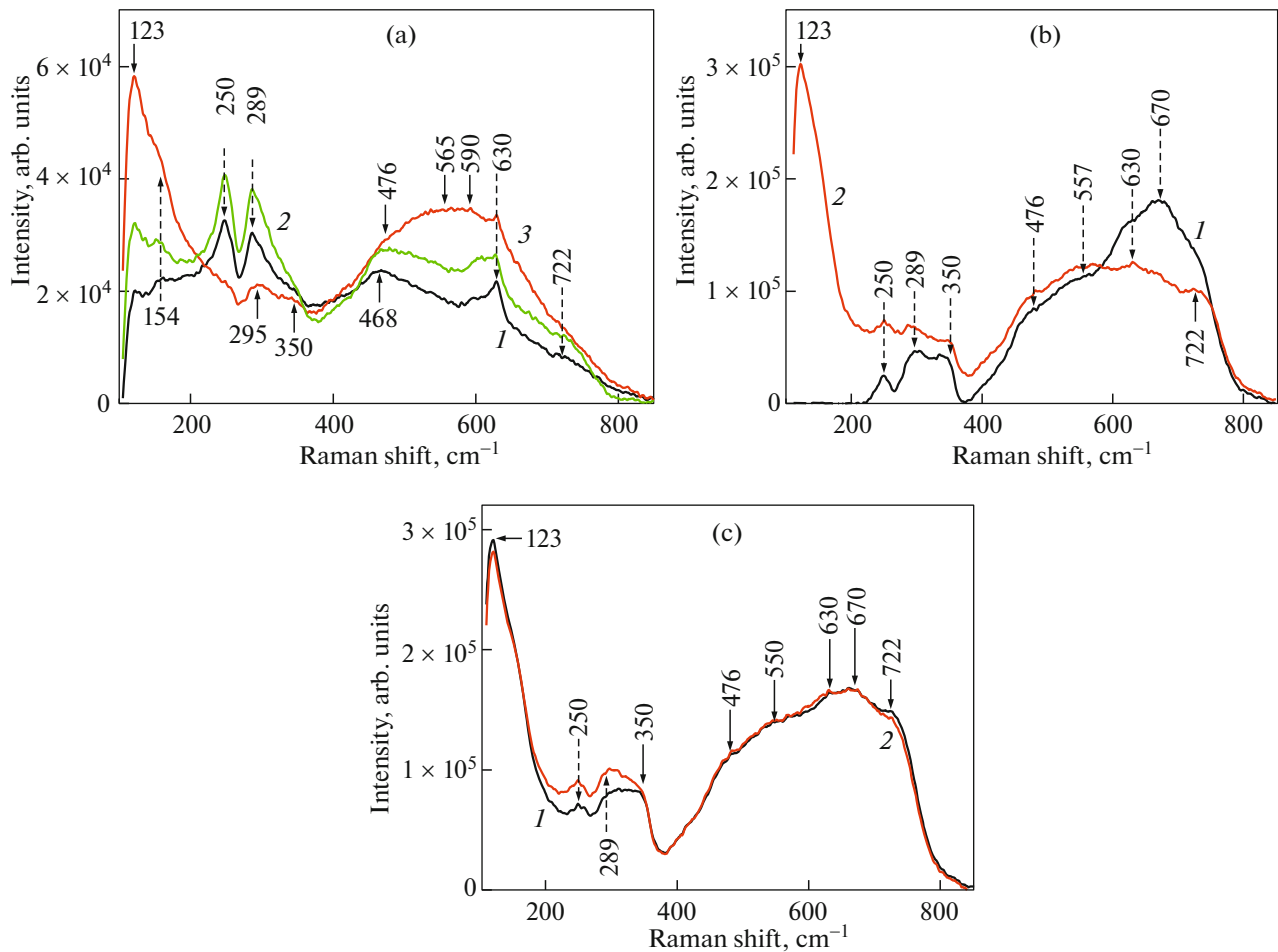


**Fig. 2.** Raman spectra of films of different compositions: (a) SnO<sub>2</sub>:Sb (curve 1), Au/SnO<sub>2</sub>:Sb (curve 2), and Pt/Pd/SnO<sub>2</sub>:Sb (curve 3); (b) (III) Au/SnO<sub>2</sub>:Sb, Au, Co; and (c) (IV) Pt/Pd/SnO<sub>2</sub>:Sb, Au, Co. Curves 1 refer to freshly prepared sensors (b, c), and curves 2 refer to the samples that have passed tests for 240 days with periodic exposure to kerosene and storage.

presence of broad bands in the ranges of 400–800 and 200–370 cm<sup>-1</sup> with a number of maxima is also recorded in a number of nanostructured SnO<sub>2</sub> materials [18–21] and is associated with size effects [21].

The presence of a dispersed Au catalyst on the surface insignificantly affects the shape of the Raman spectrum of SnO<sub>2</sub> (Fig. 2a, curve 2) [13]. Dispersed Pt/Pd layers deposited on the surface of the tin dioxide films studied in this work promote broadening and an increase in the intensity of the 400–800 cm<sup>-1</sup> band (Fig. 2a, curve 3). In addition to A<sub>1g</sub> main mode at 630 cm<sup>-1</sup>, one can distinguish not clearly pronounced maxima at 565 and 590 cm<sup>-1</sup>. The intensity of the band at 200–370 cm<sup>-1</sup> with maxima at 295 and 350 cm<sup>-1</sup> is decreased. In this case, B<sub>1g</sub> mode at 123 cm<sup>-1</sup> manifests itself as an intense maximum of the broadened band at 100–270 cm<sup>-1</sup>. It can be assumed that, for the Pt/Pd/SnO<sub>2</sub>:Sb samples (Fig. 2a, curve 3), the maxima at 565 and 590 cm<sup>-1</sup> are the result of the formation of dispersed states of Pt<sup>+2</sup> and Pd<sup>+2</sup> on the surface. The

same states can be responsible for the broadening of the band at 100–270 cm<sup>-1</sup> and an increase in the intensity of the maximum at 123 cm<sup>-1</sup>. Based on kinetic studies [22] on chemisorption, on temperature-programmed reduction [23], as well as by X-ray photoemission spectroscopy [24], it has been shown that, in platinum layers deposited on the γ-Al<sub>2</sub>O<sub>3</sub> surface, two completely different states are found. At low concentrations, the intermediate oxide PtO is present, which is identified as two-dimensional dispersed platinum in the Pt<sup>+2</sup> state. An increase in the impurity concentration is accompanied by a transition from dispersed Pt to the formation of three-dimensional particles of metallic Pt<sup>0</sup>. Pt<sup>0</sup> is inactive in Raman spectra [25], but in the presence of Pt<sup>+2</sup> in γ-Al<sub>2</sub>O<sub>3</sub> samples obtained by multiple impregnation with aqueous solutions of platinum hydrochloric acid three broad peaks were observed at 125, 335, and 590 cm<sup>-1</sup> [26]. Similar effects take place when platinum and palladium are deposited onto the surface or introduced into the bulk of tin dioxide [27].

Let us consider the Raman spectra of freshly prepared sensors from series (III) and (IV) (Figs. 2b, 2c, curves 1). It is obvious that the introduction of gold with a concentration of 1.8–1.9 at % and cobalt with a concentration of <0.3 at % into the SnO<sub>2</sub> film bulk leads to a significant change in the spectra. The intensity of the Raman spectra, which are characterized by two broadened bands in the regions of 200–400 and 400–800 cm<sup>-1</sup> with maxima at 250, 289, and 350 and 476, 630, and 722 cm<sup>-1</sup>, respectively, and which were also observed in samples without Au and Co impurities in the bulk (Fig. 2a), increases. Additional pronounced maxima appear at 670 and in the region of 550–557 cm<sup>-1</sup>. In the presence of these maxima, the spectra of the Pt/Pd/SnO<sub>2</sub>:Sb, Au, Co samples do not show the maxima at 565 and 590 cm<sup>-1</sup>, which are caused by the ultrathin layers of deposited Pt/Pd. The intensity of the Raman spectra in the Au/SnO<sub>2</sub>:Sb, Au, Co films (Fig. 2b, curve 1) with a higher Co content ( $S_{\text{Co}}/S_{\text{Sn}} = 9 \times 10^{-3}$ ) is less increased; there is no maximum at 123 cm<sup>-1</sup>. It should be noted that, in thick-film structures with a concentration of 3 and 5 vol % of Co and Fe 3d metals, a decrease in the intensity of the Raman spectra of tin dioxide was observed due to the distortion and decrease in the spatial symmetry of the lattice [28].

How does the introduction of Au, Co, and Ni impurities into the bulk of tin dioxide films affect the Raman spectra? It can be supposed that samples from series (III) and (IV) contain nanoparticles of gold in the form of a second phase, since earlier [13] we have established that the absorption spectra of Au/SnO<sub>2</sub>:Sb, Au, Ni films, which are similar to the samples from series (II) studied in this work, clearly show the bands of surface plasmon resonance (SPR) of Au. It is also seen from the absorption spectrum that the SPR of Au is blurred and significantly broadened, which indicates the formation of polydisperse nanoparticles of Au in the SnO<sub>2</sub> film.

The features of the Raman spectra of the studied films are due to an increase in the defectiveness of the crystal lattice upon the introduction of impurities (Au, Co, Ni) into the bulk of the SnO<sub>2</sub> film and are inherent in nanocrystals with violation of the long-range ordering periodicity. The Co<sup>3+</sup> and Co<sup>2+</sup> cations may be responsible for the appearance of maxima at 670 and 550–557 cm<sup>-1</sup>, which are observed in different samples from series (III) and (IV) with additions of cobalt. As has been shown by X-ray diffraction (XRD) studies of tin dioxide films with a cobalt concentration of 0.2–0.4 wt % [29] obtained using the sol–gel method and films containing 1–3 vol % of Co prepared using jet pyrolysis [30], the phases of Co oxides in the samples are not found. Based on the data of X-ray photoemission spectroscopy (XPS), the authors of [29] concluded that there are Co<sup>3+</sup> and Co<sup>2+</sup> cations on the surface of SnO<sub>2</sub> microcrystals, which form bonds with

lattice oxygen and contribute to an increase in the density of chemisorbed oxygen. Substitution of Sn by Co atoms accompanied by the appearance of interstitial Sn<sub>i</sub> is also possible [31, 32].

Analysis of the Raman spectra of sensors after long-term tests under the influence of kerosene (Figs. 2b, 2c, curves 2) indicates that the position of the main modes remained unchanged. In the case of Pt/Pd/SnO<sub>2</sub>:Sb, Au, Co samples, the intensity of the spectra did not change either. For Au/SnO<sub>2</sub>:Sb, Au, Co films from series (III) with an increased cobalt content, the spectrum intensity in the range of 580–740 cm<sup>-1</sup> decreased, the intensity of the 200–400 cm<sup>-1</sup> band increased, and a maximum appeared at 123 cm<sup>-1</sup>. The established regularities are consistent with the concepts of [17, 32, 33], according to which the Raman spectra of nanocrystalline metal oxides contain information not only about different sizes of crystallites, but also about the structure and chemical composition of thin films, as well as the catalytic properties of the surface.

## 2.2. Study of Gas-Sensitive Characteristics of Sensors

The principle of operation of sensors based on tin dioxide is as follows [11]. Oxygen chemisorption occurs on the SnO<sub>2</sub> surface in the atmosphere. The oxygen molecule captures an electron from the conduction band of the semiconductor and becomes charged negatively. In the near-surface region of tin dioxide, a space charge region (SCR) that is depleted in electrons with a width of  $d_0$  is formed, while the conductivity of the semiconductor film decreases. The molecular form of oxygen O<sub>2</sub><sup>-</sup> prevails at low temperatures of <200°C. At higher temperatures, oxygen is adsorbed in the form of O<sup>-</sup>, which is most active in the reactions of oxidation of reducing gases (hydrogen, carbon monoxide, hydrocarbons, etc.) on the surface of SnO<sub>2</sub> and provides the maximum response in the temperature range of 350–450°C. TS-1 aviation kerosene is a mixture of hydrocarbons including alkanes (58.7–62.2%), cycloalkanes (21.4–24.4%), arenes (15.4–16.2%), and olefins (0.7–1.0%). Studies of reactions during the oxidation of kerosene in air [34, 35], as well as on the surface of thick-film samples of tin dioxide [36], have shown that in all cases the dissociation of hydrocarbon molecules occurs with the release of atomic hydrogen, which is capable of interacting with the surface of the metal oxide sensor. The formation of complex products of the reaction, such as phenol C<sub>6</sub>H<sub>5</sub>OH and butylene C<sub>4</sub>H<sub>8</sub>, takes place [35, 36].

Higher resistance values in clean air  $R_0 = 7–12 \text{ M}\Omega$  (Table 1) are characteristic of sensors from series (I) and (IV) with dispersed catalytic Pt/Pd layers deposited on the surface of tin dioxide, which contribute to an increase in the density of chemisorbed oxygen and increase in the width of the SCR. In the presence of

**Table 1.** Values of resistance in clean air  $R_0$  and response to 15 ppm of aviation kerosene vapors of sensors that were freshly prepared and tested for a month from various series

Type of sensor	Before tests		After tests	
	$R_0$ , M $\Omega$	$G_1/G_0$	$R_0$ , M $\Omega$	$G_1/G_0$
(I) Pt/Pd/ SnO <sub>2</sub> :Sb	7.2–9.0	2.6–2.8	3.6–3.9	1.1–1.2
(II) Au/SnO <sub>2</sub> :Sb, Au, Ni	2.8–3.4	2.2–2.5	1.2–1.4	2.9–3.1
(III) Au/SnO <sub>2</sub> :Sb, Au, Co	4.6–5.1	2.5–2.6	5.1–5.4	2.7–3.1
(IV) Pt/Pd/SnO <sub>2</sub> :Sb, Au, Co	7.1–9.0	2.7–2.8	2.6–3.0	3.1–3.2

The measurements were performed at  $T = 450^\circ\text{C}$ .

gold in the bulk and on the surface of tin dioxide films, the probability of oxygen chemisorption is lower; therefore, the negative charge density decreases. As was shown earlier [11, 12], the resistance for the Au/SnO<sub>2</sub>:Sb, Au sensors is  $R_0 = 0.23\text{--}0.30$  M $\Omega$ . The introduction of Ni and Co into the bulk of gold-modified thin films promotes an increase in  $R_0$  in samples from series (II) and (III), and the higher values of resistance  $R_0$  compared to films from series (II) correspond to a higher Co content in films from series (III). These regularities are consistent with the features of the Raman spectra of the samples, as well as with earlier-obtained data [12, 13, 28–33], and confirm the notion that, upon crystallization of the studied thin films, as well as films obtained using thick-film technology, during thermal annealing, 3d-metal atoms in the volume of SnO<sub>2</sub> partially segregate on the surface of microcrystals and form bonds with lattice oxygen; metal cations are formed (for example, Co<sup>3+</sup> and Co<sup>2+</sup>), as well as atoms of interstitial nonstoichiometric tin, which are the centers of oxygen adsorption on the

SnO<sub>2</sub> surface and contribute to an increase in the resistance of the sensors.

The study of the temperature dependences of the response of freshly prepared sensors to the effect of 15 ppm of aviation kerosene vapor (Fig. 3) showed that  $G_1/G_0$  of sensors with a dispersed gold layer deposited on the surface (series (II) and (III)) monotonically increase with increasing temperature up to 450°C. The responses of sensors with Pd and Pt layers deposited on the surface reach maximum values at temperatures of 350 (series (IV)) and 400°C (series (I)), and change insignificantly with a further increase in temperature, since it is known [11] that Pt/Pd catalysts reduce the temperature of dissociative adsorption of molecular hydrogen and, apparently, vapors of liquid hydrocarbons. Temperatures of 430–450°C were chosen as working temperatures, at which all sensors had sufficiently high  $G_1/G_0$  values (Table 1) and short response times  $t_r = 3\text{--}4$  s.

For a preliminary study of the stability of the sensor parameters, the dependences of the response on the concentration of kerosene vapors in the range of 5–75 ppm were measured in the constant heating mode for a month with an interval of 2–4 days. After prolonged exposure to vapors, the responses of sensors with 3d-metal additives (series (II)–(IV)) remained practically unchanged, whereas for sensors from series (I) they significantly decreased after 30 days of testing (Table 1). The values of resistances in clean air  $R_0$  decreased for all sensors in the course of testing. It should be noted that, with prolonged exposure to molecular hydrogen, an increase in the resistance and response to hydrogen of sensors based on tin dioxide is observed [11]. This is due to the fact that atomic hydrogen released during dissociative adsorption of H<sub>2</sub> is capable of interacting with lattice oxygen and partially reducing the tin dioxide molecules emerging on the surface. As a result, the density of superstoichiometric tin atoms, which are the centers of oxygen adsorption, increases. The decrease in resistance and response under prolonged exposure to aviation kerosene vapors can be explained by the fact that dissociation of hydrocarbons contained in kerosene vapors, along with the release of atomic hydrogen, is accom-

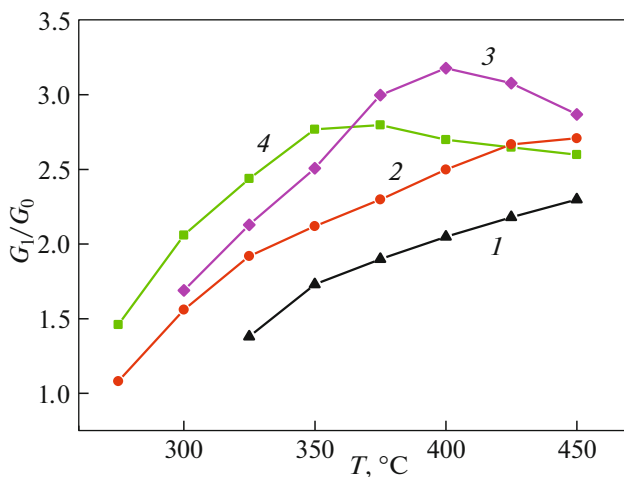


**Fig. 3.** Dependences on the operating temperature of the response to 15 ppm of kerosene of freshly prepared sensors from the series: curve 1—(II), curve 2—(III), curve 3—(IV), and curve 4—(I).

panied by the formation of complex products of the reaction that can be accumulated on the surface of  $\text{SnO}_2$ . In addition, saturated hydrocarbons can be adsorbed on the semiconductor surface, which also block the oxygen adsorption centers. Since a significant decrease in the response is observed only for sensors from series (I), it can be supposed that gold and 3d-metal additives introduced into the bulk of the films partially prevent the blocking of adsorption centers on the  $\text{SnO}_2$  surface. Therefore, to create sensors for kerosene vapors, the samples from series (II)–(IV) were selected for further studies.

The dependences of the responses of the tested sensors on the concentration of kerosene vapors are power-law (Fig. 4) and correspond to the expression

$$G_1 = \alpha n^m, \quad \log G_1 = \log \alpha + m \log n. \quad (1)$$

The values of parameter  $m$  for all freshly prepared sensors are 0.36–0.39 and increase to 0.46–0.55 after testing. The sensor response to 45 ppm of vapors is  $G_1/G_0 = 3$ –4. At the same time, the sensors can detect kerosene vapor at a level of 5 ppm, which corresponds to 0.1 PEL.

In addition, it is of interest to consider the characteristics of sensors in the thermal cycling mode. Studies [11–14] of Pt/Pd/ $\text{SnO}_2$ :Sb and Au/ $\text{SnO}_2$ :Sb, Au, Ni thin-film sensors under the influence of such reducing gases as hydrogen, carbon monoxide, and hydrogen sulfide showed that a significant increase in the response is observed under certain modes of thermal cycling, which implies a change in the operating temperature of the sensors according to a certain law. A heating cycle to temperatures of  $T_2 = 400$ – $450^\circ\text{C}$  is necessary for desorption of the products of the interaction of gas molecules with the sensor surface and release of adsorption centers, on which oxygen is chemisorbed in the form of  $\text{O}^-$ . In the cooling cycle at  $T_1$ , the processes of gas adsorption and its oxidation by active atomic oxygen accumulated in the heating cycle prevail.

In thin films of tin dioxide modified with the considered catalysts, during the transition between crystallites, the electron must overcome the potential barrier, height  $e\phi_s$  of which is proportional to the density of chemisorbed oxygen [11]. According to [11, 14], the value of  $e\phi_s$  can be determined by the formula

$$e\phi_s = [kT_1T_2/(T_2 - T_1)] \times \ln[(G_0(T_2)/G_0(T_1))(T_2/T_1)^{0.75}] + kT_2, \quad (2)$$

where  $k$  is the Boltzmann constant, if the stationary values of  $G_0$  are measured in the thermal cycling mode for two different values of the sensor temperature, but at the same  $e\phi_s$ .

For this purpose, temperature  $T_2$  and duration  $t_2$  of the heating cycle should be selected in such a way that the stationary values of  $e\phi_s(T_2)$  and  $G_0(T_2)$  are established by the end of this cycle. In the cooling cycle,

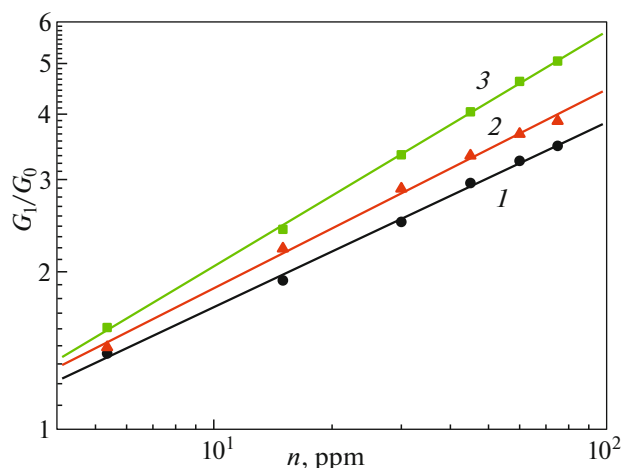
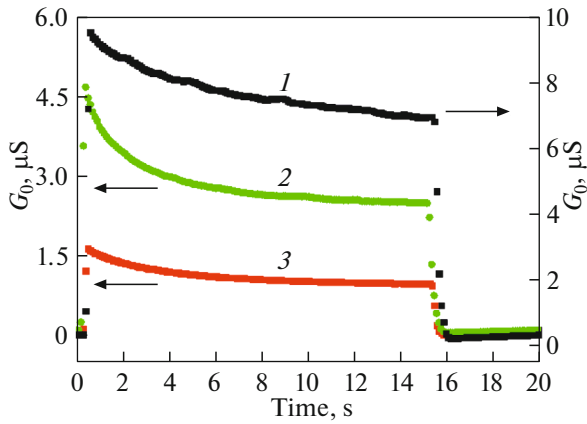


Fig. 4. The concentration dependences of the response measured at an operating temperature of  $450^\circ\text{C}$  after testing sensors from the series: curve 1—(II), curve 2—(III), and curve 3—(IV).

sensor temperature  $T_1$  should be significantly lower, so that for some time after a rapid decrease in temperature from  $T_2$  to  $T_1$  oxygen ion density on the surface  $N_s(T_2)$  and energy band bending  $e\phi_s(T_2)$  are maintained. At the same time, the condition  $T_1 \geq 200^\circ\text{C}$  must be satisfied for  $\text{O}^-$  ions to be adsorbed on the  $\text{SnO}_2$  surface. Based on the results of preliminary studies for samples from series (II)–(IV), the following thermal cycling modes were selected:  $T_2 = 450^\circ\text{C}$  ( $t_2 = 15$  s) and  $T_1 = 200^\circ\text{C}$  ( $t_1 = 5$  s). Time dependences of the conductivity  $G_0(t)$  shown in Fig. 5 satisfy the requirements, the fulfillment of which is necessary to determine the energy band bending at the grain boundaries of tin dioxide. For all freshly prepared sensors, the  $e\phi_s$  values are 0.51–0.56 eV. In Au/ $\text{SnO}_2$ :Sb, Au films without additives of 3d-metals with a reduced density of oxygen adsorption centers [11], energy band bending  $e\phi_s = 0.23$ – $0.26$  eV is much lower.

The measurement of responses to the action of kerosene vapors was carried out at the end of the heating  $S(T_2)$  and cooling  $S(T_1)$  cycles at temperatures  $T_2$  and  $T_1$  selected above. The choice of durations  $t_2$  and  $t_1$  to obtain the maximum response values required additional research, as a result of which it was shown that  $t_1 = 5$  s and  $t_2 = 10$  s are necessary. The nature of the conductivity–time profiles (CTPs) of sensors from all series in the selected thermal cycling mode is practically the same; CTPs in clean air and when exposed to kerosene vapors are compared in Fig. 6 using a sample from series (IV) as an example. It was found that the responses in the heating cycle  $S(T_2) = 2.3$ – $2.8$  practically do not differ from the  $G_1/G_0$  values measured in the constant heating mode (Table 1), which is also typical for other earlier studied sensors [11–13]. In the cooling cycle, the responses are  $S(T_1) = 4.6$ – $9.8$ , i.e.,



**Fig. 5.** Conductivity–time profiles in the thermal cycling mode in clean air for sensors from the series: curve 1—(II) Au/SnO<sub>2</sub>:Sb, Au, Ni, curve 2—(III) Au/SnO<sub>2</sub>:Sb, Au, Co, and curve 3—(IV) Pt/Pd/SnO<sub>2</sub>:Sb, Au, Co.

2–2.5 times higher. It should be noted that, when using pulsed heating in the case of sensors for simple reducing gases, such as H<sub>2</sub>, CO, and H<sub>2</sub>S [11], the response values in the cooling cycle are several times higher—and, at high gas concentrations, one or two orders of magnitude higher—than the values measured in the heating cycle. It can be assumed that complex products of oxidation of aviation kerosene vapors are not completely desorbed from the semiconductor surface during the heating cycle. This is also evidenced by a decrease in the response values both in the heating cycle and in the cooling cycle with a decrease in the heating cycle duration  $t_2 < 10$  s.

After testing the sensors from series (II)–(IV) carried out for a month the samples were stored in Petri dishes in laboratory air for 180 days. Then, for 60 days with an interval of 10 days in the modes of constant and pulsed heating, the parameters of the samples were measured under the action of aviation kerosene vapors. Table 2 shows the characteristics of the sensors after all tests were completed. Obviously, in contrast to samples from series (I), for which the response to ker-

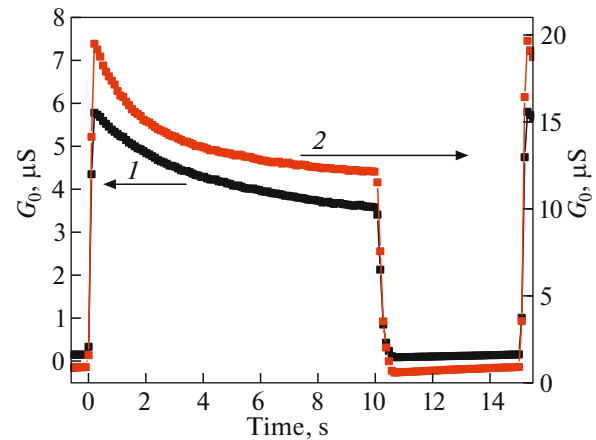


**Fig. 6.** Conductivity–time profiles of the (IV) Pt/Pd/SnO<sub>2</sub>:Sb, Au, Co sensor: curve 1 in clean air, and curve 2 under the influence of 15 ppm of kerosene vapor.

osene vapor decreased to 1.1–1.2 during the process of preliminary tests for a month (Table 1), the values of  $R_0$  and responses of sensors with Ni and Co additives measured in the modes of constant and pulsed heating changed insignificantly after long-term tests (Table 2).

The bends bending at grain boundaries in tin dioxide decreased in the case of samples from series (II) with minimal concentrations of Au and Co in the volume and increased for sensors from series (III) with an increased content of these additives, primarily of Co. Herewith, the response time increased for samples from series (II) and (III) with a dispersed layer of gold deposited on the surface. The change in the state of the surface of the Au/SnO<sub>2</sub>:Sb, Au, Co sensors is also evidenced by the presence of features of the Raman spectra (Fig. 2b). Sensors from series (IV) are characterized by the highest performance, as well as stable values of  $e\varphi_s$  and other parameters after long-term tests. According to Raman spectroscopy data, a slight increase in the intensity of the 200–400 cm<sup>-1</sup> band (Fig. 2c) corresponds to an insignificant change in the

**Table 2.** The main parameters of kerosene sensors from various series after completion of all tests for 240 days

Type of sensor	(II) Au/SnO <sub>2</sub> :Sb, Au, Ni	(III) Au/SnO <sub>2</sub> :Sb, Au, Co	(IV) Pt/Pd/SnO <sub>2</sub> :Sb, Au, Co
$R_0, M\Omega$	1.4–2.3	4–7	3–4
$G_1/G_0$	1.8–1.9	2.2–2.6	2.2–2.7
$t_r, s$	30–40	20–22	12–14
$S(T_1)$	4.9–6.6	6.2–9.8	5.3–7.9
$S(T_2)$	2.4–2.6	2.5–3.0	2.6–2.8
$e\varphi_s, eV$	0.46–0.50	0.59–0.61	0.52–0.54

Values of  $R_0$ , response  $G_1/G_0$ , and response time  $t_r$  were measured at an operating temperature of 450°C.  $S(T_1)$  and  $S(T_2)$  were measured in optimal thermal cycling modes. All responses and  $t_r$  correspond to the kerosene vapor concentration of  $n = 15$  ppm.



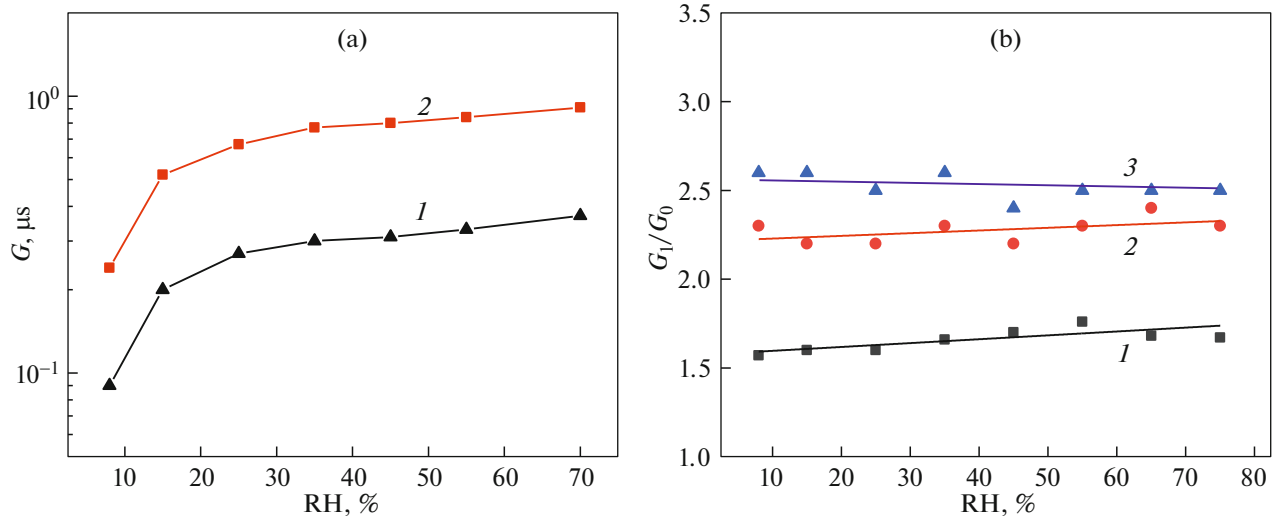


Fig. 7. Dependences on the level of humidity: (a) conductivity in clean air  $G_0$ , curve 1, and when exposed to 15 ppm of kerosene vapor  $G_1$ , curve 2; (b) response to 15 ppm of kerosene vapor of sensors from the series: curve 1—(II), curve 2—(III), and curve 3—(IV).

structure and composition of the Pt/Pd/SnO<sub>2</sub>:Sb, Au, Co films.

One source of instability of the parameters of sensors based on metal oxide semiconductors is the change in the humidity of the environment [11]. Upon adsorption, a water molecule dissociates into the hydroxyl group OH<sup>-</sup> and proton H<sup>+</sup>. The proton is captured by the O<sup>-</sup> ion forming a neutral OH group. After neutralization of the OH<sup>-</sup> group (the electron passes into the conduction band of SnO<sub>2</sub>), both hydroxyl groups can be desorbed, the density of chemisorbed oxygen decreases, and the values of the response to reducing gases, as a rule, decrease with an increase in the humidity level.

For the films studied in this work, the values of conductivity  $G_0$  in pure air and  $G_1$  in an environment containing kerosene vapors grow at the same rate in dry air with an increase in RH from 8 to 25% and then change insignificantly under conditions of real humidity (Fig. 7a). The magnitude of the  $G_1/G_0$  response is weakly dependent on humidity in a wide range of RH (Fig. 7b).

## CONCLUSIONS

The results of the research showed that, to create sensors for low concentrations of liquid hydrocarbon vapors (5–75 ppm of aviation kerosene), it is advisable to use thin nanocrystalline tin dioxide films obtained by magnetron sputtering with dispersed Pt/Pd or Au catalysts deposited on the surface and additives of gold and 3d-metals (Ni, Co) introduced into the bulk. An increase in the response to the effect of hydrocarbon vapors by 2–2.5 times is provided by using the thermal cycling mode at certain temperatures and the durations of the heating and cooling cycles.

Based on the results of comprehensive studies of the structure, composition, and properties of films, possible processes of interaction of aviation kerosene molecules with the SnO<sub>2</sub> surface and degradation of sensor parameters were considered depending on the type of catalysts in the bulk and on the surface. It was established by laser Raman spectroscopy that the deposition of dispersed Pt/Pd layers on the surface and, in particular, the introduction of gold and 3d-metal additives into the bulk of the films leads to the appearance of additional modes in the Raman spectra that are absent in the samples without impurities, which is associated with local symmetry breaking and dimensional effects. After long-term tests of sensors, the position of all modes did not change, which indicates a high stability of the structure and composition of the films. In the case of Pt/Pd/SnO<sub>2</sub>:Sb, Au, Co samples, the intensity of the spectra did not change either. Changes in the intensity of the maxima in different regions of the Raman spectrum for the Au/SnO<sub>2</sub>:Sb, Au, Co films reflect, apparently, some transformations on the surface, which lead to an increase in the response time of the sensors.

Pt/Pd/SnO<sub>2</sub>:Sb, Au, Co sensors, being characterized by high performance, stable values of the bend at the grain boundaries of tin dioxide  $e\varphi_s$  and response to the effect of trace concentrations of aviation kerosene after long-term tests and under conditions of varying humidity, can be successfully used to detect liquid vapors of hydrocarbons.

## FUNDING

This work was carried out with support of the Program for Competitiveness Enhancement of Tomsk State University.

## CONFLICT OF INTEREST

The authors declare that they have no conflicts of interest.

## REFERENCES

- Q. Dong, H. Su, D. Zhang, and F. Zhang, *Nanotechnology* **17** (15), 3968 (2006).  
<https://doi.org/10.1088/0957-4484/17/15/060>
- Y. Zong, Y. Cao, and D. Jia, *Sens. Actuators, B* **145** (1), 84 (2010).  
<https://doi.org/10.1016/j.snb.2009.11.026>
- A. A. Vasiliev and V. V. Malyshev, *Sens. Actuators, B* **189**, 260 (2013).  
<https://doi.org/10.1016/j.snb.2013.07.047>
- G. Korotcenkov, *Mater. Sci. Eng., B* **139**, 1 (2007).
- A. Cabot, A. Dieguez, A. Romano-Rodríguez, J. R. Morante, and N. Bárzan, *Sens. Actuators, B* **79**, 98 (2001).
- M. N. Rumyantseva and A. M. Gas'kov, *Russ. Chem. Bull.* **57**, 1106 (2008).  
<https://doi.org/10.1007/s11172-008-0139-z>
- G. Korotcenkov and B. K. Cho, *Sens. Actuators, B* **244**, 182 (2017).  
<https://doi.org/10.1016/j.snb.2016.12.117>
- G. Korotcenkov and B. K. Cho, *Sens. Actuators, B* **156**, 527 (2011).  
<https://doi.org/10.1016/j.snb.2011.02.024>
- I. Lee, S.-J. Choi, K. M. Park, S. S. Lee, S. Choi, I.-D. Kim, and C. O. Park, *Sens. Actuators, B* **197**, 300 (2014).  
<https://doi.org/10.1016/j.snb.2014.02.043>
- T. Itoh, I. Matsubara, M. Kadosaki, Y. Sakai, W. Shin, and N. Izu, *Sensors* **10**, 6513 (2010). <https://www.mdpi.com/1424-8220/10/7/6513>
- N. K. Maksimova, E. Yu. Sevast'yanov, N. V. Sergeichenko, and E. V. Chernikov, *Semiconductor Thin-Film Gas Sensors* (NTL, Tomsk, 2016) [in Russian].
- E. Yu. Sevast'yanov, N. K. Maksimova, A. I. Potekaev, N. V. Sergeichenko, E. V. Chernikov, A. V. Almaev, and B. O. Kushnarev, *Russ. Phys. J.* **60** (7), 1094 (2017).  
<https://doi.org/10.1007/s11182-017-1184-6>
- N. K. Maksimova, A. A. Biryukov, E. Yu. Sevast'yanov, and E. V. Chernikov, *Russ. J. Appl. Chem.* **93**, 427 (2020).  
<https://doi.org/10.1134/S1070427220030155>
- N. K. Maksimova, A. V. Almaev, E. Y. Sevastyanov, A. I. Potekaev, E. V. Chernikov, N. V. Sergeychenko, P. M. Korusenko, and S. N. Nesov, *Coatings* **9** (7), 423 (2019).  
<https://doi.org/10.3390/coatings9070423>
- A. Dieguez, A. Romano-Rodríguez, A. Vilá, and J. R. Morante, *J. Appl. Phys.* **90** (3), 1550 (2001).  
<https://doi.org/10.1063/1.1385573>
- G. Singh, R. Thangaraj, and R. C. Singh, *Ceram. Int.* **42** (3), 4323 (2016).  
<https://doi.org/10.1016/j.ceramint.2015.11.111>
- M. Zheng, G. Li, X. Zhang, S. Huang, Y. Lei, and L. Zhang, *Chem. Mater.* **13** (11), 3859 (2001).  
<https://doi.org/10.1021/cm010084q>
- M. Ristic, M. Ivanda, S. Popovic, and S. Music, *J. Non-Cryst. Solids* **303** (2), 270 (2002).  
[https://doi.org/10.1016/S0022-3093\(02\)00944-4](https://doi.org/10.1016/S0022-3093(02)00944-4)
- M. Ocaña, C. J. Serna, J. V. Garcia-Ramos, and E. Matijevic, *Solid State Ionics* **63**, 170 (1993).  
[https://doi.org/10.1016/0167-2738\(93\)90102-9](https://doi.org/10.1016/0167-2738(93)90102-9)
- K. N. Yu, Y. Xiong, Y. Liu, and C. Xiong, *Phys. Rev. B* **55** (4), 2666 (1997).  
<https://doi.org/10.1103/PhysRevB.55.2666>
- M. N. Rumyantseva, A. M. Gaskov, N. Rosman, T. Pagnier, and J. R. Morante, *Chem. Mater.* **17** (4), 893 (2005).  
<https://doi.org/10.1021/cm0490470>
- H. C. Yao, H. S. Gandhi, and M. Shelef, *Stud. Surf. Sci. Catal.* **11**, 159 (1982).
- H. C. Yao, M. Sieg, and H. K. Plummer, *J. Catal.* **59**, 365 (1979).
- J. Z. Shyu, and K. Otto, *Appl. Surf. Sci.* **32** (1–2), 246 (1988).  
[https://doi.org/10.1016/0169-4332\(88\)90085-2](https://doi.org/10.1016/0169-4332(88)90085-2)
- G. W. Graham, W. H. Weber, J. R. McBride, and C. R. Peters, *J. Raman Spectrosc.* **22**, 1 (1991).
- K. Otto, W. H. Weber, G. W. Graham, and J. Shyu, *Appl. Surf. Sci.* **37** (2), 250 (1989).  
[https://doi.org/10.1016/0169-4332\(89\)90487-X](https://doi.org/10.1016/0169-4332(89)90487-X)
- A. Cabot, A. Dieguez, A. Romano-Rodríguez, J. R. Morante, and N. Barsan, *Sens. Actuators, B* **79** (2–3), 98 (2001).  
[https://doi.org/10.1016/S0925-4005\(01\)00854-1](https://doi.org/10.1016/S0925-4005(01)00854-1)
- J. Kaur, J. Shah, R. K. Kotnala, and K. Ch. Verma, *Ceram. Int.* **38** (7), 5563 (2012).  
<https://doi.org/10.1016/j.ceramint.2012.03.075>
- L. P. Oleksenko, N. P. Maksymovych, A. I. Buvailo, I. P. Matushko, and N. Dollahon, *Sens. Actuators, B* **174**, 39 (2012).  
<https://doi.org/10.1016/j.snb.2012.07.079>
- G. Korotcenkov, I. Boris, V. Brinzari, S. H. Han, and B. K. Cho, *Sens. Actuators, B* **182**, 112 (2013).  
<https://doi.org/10.1016/j.snb.2013.02.103>
- L. Liu, C. Guo, S. Li, L. Wang, Q. Dong, and W. Li, *Sens. Actuators, B* **150**, 806 (2010).  
<https://doi.org/10.1016/j.snb.2010.07.022>
- S. Roy, A. G. Joshi, S. Chatterjee, and A. K. Ghosh, *Nanoscale* **10** (22), 10664 (2018).  
<https://doi.org/10.1039/c7nr07427a>
- M. A. Bañares and I. E. Wachs, *J. Raman Spectrosc.* **33** (5), 359 (2002).  
<https://doi.org/10.1002/jrs.866>
- A. M. Starik, N. S. Titova, and S. A. Torokhov, *Combust., Explos. Shock Waves* **49** (4), 392 (2013).  
<https://doi.org/10.1134/S0010508213040023>
- L. Q. Maurice, J. W. Blust, K. L. Leung, and R. P. Lindstedt, *Proc. 37th AIAA Aerospace Sciences Meeting and Exhibit, Reno, Nevada, January 11–14, 1999*, AIAA 99-1038.  
<https://doi.org/10.2514/6.1999-1038>
- M. C. Carotta, V. Guidi, G. Martinelli, and M. Nagliati, *Sens. Actuators, B* **130** (1), 497 (2008).  
<https://doi.org/10.1016/j.snb.2007.09.053>

Translated by S. Rostovtseva